ACS Medicinal Chemistry Letters

Letter

Pyridinylimidazoles as GSK3# inhibitors: the impact of tautomerism on compound activity via water networks

Fabian Heider, Tatu Pantsar, Mark Kudolo, Francesco Ansideri, Angela De Simone, Letizia Pruccoli, Taiane Schneider, Marcia Inês Goettert, Andrea Tarozzi, Vincenza Andrisano, Stefan A. Laufer, and Pierre Koch

ACS Med. Chem. Lett., **Just Accepted Manuscript** • DOI: 10.1021/acsmedchemlett.9b00177 • Publication Date (Web): 26 Aug 2019

is published by the American Chemical Society. 1155 Sixteenth Street N.W., Washington, DC 20036

Pyridinylimidazoles as GSK3β inhibitors: the impact of tautomerism on compound activity via water networks

Fabian Heider[†#], Tatu Pantsar[‡§#], Mark Kudolo[†], Francesco Ansideri[†], Angela De Simone[∥], Letizia Pruccoli[∥], Taiane Schneider[▽], Marcia Inês Goettert[▽], Andrea Tarozzi[∥], Vincenza Andrisano[∥], Stefan A. Laufer[†], Pierre Koch[†⊥*]

[†]Department of Pharmaceutical and Medicinal Chemistry, Institute of Pharmaceutical Sciences, Eberhard Karls Universität Tübingen, Auf der Morgenstelle 8, 72076 Tübingen, Germany.

[‡]School of Pharmacy, University of Eastern Finland, P.O.BOX 1627, 70211 Kuopio, Finland.

[§] Department of Internal Medicine VIII, University Hospital Tübingen, Otfried-Müller-Straße 14, 72076 Tübingen, Germany.

[∥]Department for Life Quality Studies, Alma Mater Studiorum-University of Bologna, Corso D'Augusto, 237, 47921 Rimini, Italy.

[▽]Cell Culture Laboratory, Postgraduate Program in Biotechnology, University of Vale do Taquari (Univates), Lajeado, Brazil

[⊥]Department of Pharmaceutical/Medicinal Chemistry II, Institute of Pharmacy, University of Regensburg, Universitätsstraße 31, 93053 Regensburg, Germany.

KEYWORDS. Protein Kinase Inhibitors; Glycogen Synthase Kinase-3β; Pyridinylimidazoles; Tautomerism; Molecular Dynamics Simulation; Quantum Mechanics.

ABSTRACT: Glycogen synthase kinase-3β (GSK3β) is involved in many pathological conditions and represents an attractive drug target. We previously reported dual GSK3β/p38α mitogen-activated protein kinase inhibitors and identified *N*-(4-(4-(4-fluorophenyl)-2-methyl-1*H*-imidazol-5-yl)pyridin-2-yl)cyclopropanecarboxamide (**1**) as a potent dual inhibitor of both target kinases. In this study, we aimed to design selective GSK3β inhibitors based on our pyridinylimidazole scaffold. Our efforts resulted in several novel and potent GSK3β inhibitors with IC_{50} values in the low nanomolar range. 5-(2-(Cyclopropanecarboxamido)pyridin-4-yl)-4-cyclopropyl-1*H*-imidazole-2-carboxamide (**6g**) displayed very good kinase selectivity as well as metabolically stability and inhibits GSK3β activity in neuronal SH-SY5Y cells. Interestingly, we observed the importance of the 2-methylimidazole's tautomeric state for the compound activity. Finally, we reveal how this crucial tautomerism effect is surmounted by imidazole-2-carboxamides, which are able to stabilize the binding via enhanced water network interactions, regardless of their tautomeric state.

Glycogen Synthase Kinase 3β (GSK3β) is a ubiquitously expressed serine/threonine kinase, which plays an important role in a variety of different cell signaling pathways. GSK3β plays a crucial role in almost every pathway leading to the hallmarks of Alzheimer's disease[1-2] and is often referred to as a tau-kinase due to its capacity to modulate tau hyperphosphorylation. Overactivity of GSK3β has also been connected to an increased production of β-amyloids,[3] neuroinflammation and oxidative stress.[4]

GSK3β has also been associated with a plethora of other pathological conditions such as diabetes,[5] cancer,[6-8] schizophrenia,[9] bipolar disorders[10] and osteoporosis.[11] Thus, GSK3β is considered to be an attractive drug target.

We recently reported a series of pyridinylimidazoles as dual GSK3β/ p38α MAP kinase (MAPK) inhibitors and identified trisubstituted imidazole **1** as a potent balanced inhibitor of both target enzymes (*Figure 1*).[12] Furthermore, we observed that the removal of the *para*-fluorophenyl ring (**2**), which might be located in the hydrophobic region (HR) I of the ATP binding site, resulted in a significantly reduced GSK3β inhibition with a complete loss of activity against p38α MAPK. In this study, our aim was to further improve the activity of our pyridinylimidazole scaffold while shifting the selectivity towards GSK3β.

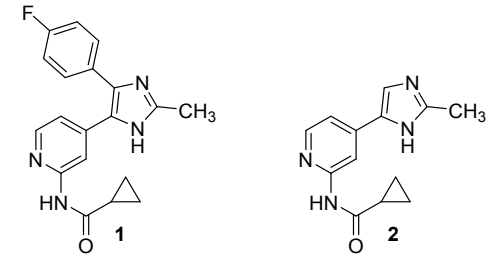

IC_{50} (GSK3β) = 0.053 μM
IC_{50} (p38α) = 0.019 μM

IC_{50} (GSK3β) = 1.68 μM
IC_{50} (p38α) > 10 μM

Figure 1. Pyridinylimidazole-based lead compounds **1** and **2**.

Recently, employing quantum mechanics (QM) to drug design and development has become increasingly popular. For instance, QM can be utilized to improve docking and scoring, determining protonation states and optimizing structures as well as ligand binding energies.[13-14] Also, the importance of water in drug design is gaining more and more emphasis.[15] The effect of water network stabilization for ligand binding has been demonstrated e.g. by Klebe and coworkers.[16] In addition, molecular dynamics (MD) simulations offer valuable insights into ligand binding interactions.[17] By utilizing QM calculations with MD simulations we disclosed the importance of tautomerism and water networks for the activity of our pyridinylimidazole compounds. In this case, the observed SAR could not have been clarified by simplified computational tools, such as docking, which has major caveats especially related to the solvent effects and dynamics of the system[18] that were found determining for the activity differences among imidazoles.

Results and discussion

Detailed descriptions of the synthetic sequences are reported in *Schemes S1-S14* (Supporting Information, SI).

To address the alarming diffuse trend of increasing the inhibitor logP value in the lead optimization,[19] we monitored the lipophilic ligand efficacy (LLE) of the synthesized compounds.[20] The LLE of our lead compounds **1** and **2** was already high with values of 5.10 and 4.40, respectively (*Table 1*).

Initially, we examined the influence of different substituents reaching into the HR I of GSK3β. To this end, we synthesized a series of 2-methylpyridinylimidazoles with different (cyclo)aliphatic and aromatic moieties attached to the imidazole-C4 position.

Replacing the aromatic ring with cycloalkyl moieties at the imidazole-C4 position (**3j-m**) resulted in a substantial loss of activity, leading to modest inhibitors of GSK3β in the micromolar range displaying complete inactivity against p38α MAPK.

Compounds with bulky moieties, such as 2-naphtyl (**3h**), were inactive, probably because of a steric clash in the HR I.

Replacement of the *para*-fluorophenyl ring with the 5-membered heteroaromatic rings thiophene (**3d**) or furan (**3e**) as well as other minor changes on the *para*-fluorophenyl ring, such as addition of a methyl (**3o**) or a second fluorine atom (**3i**), led to inhibitors with slightly increased IC_{50} values compared to **1**. Introduction of a pyrimidine (**3g**) at the imidazole-C4 led to a completely inactive derivative. The less lipophilic *ortho*- and *meta*-hydroxyphenyl derivatives (**3a** and **3b**, respectively) turned out to be potent GSK3β inhibitors with sound LLE values, while the *para*-hydroxyphenyl compound (**3c**) displayed substantially diminished inhibition against both kinases. All potent GSK3β inhibitors bearing an aromatic ring in the HR I, however, remained potent inhibitors of p38α MAPK, except for **3e** with 10-fold selectivity for GSK3β.

To elucidate the observed dramatic loss of activity of certain compounds, we investigated the influence of the R_1-substituent on the imidazole ring's tautomeric state. To this end, we conducted QM calculations to assess the probability of different tautomeric states and conformations for the compounds (*Figure 2, see SI for details*). Indeed, QM results indicated that the active compounds generally prefer the tautomer A or at least represent a reasonable population of this tautomeric state (*Table S3*). For instance, the low nanomolar inhibitors **3a**, **3b**, **3d** and **3e**, display a clear preference for tautomer A (>71.5%). In turn, the Less active compounds **3c** and **3j-m**, display a clearly diminished population of tautomer A (<17%).

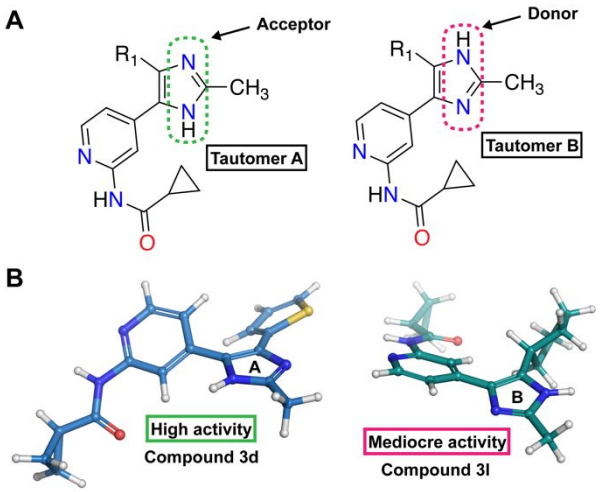

Figure 2. (**A**) The imidazole ring has two potential tautomeric forms: in tautomer A, the nitrogen next to the R_1-group is unprotonated and can act as a H-bond acceptor, whereas in tautomer B it is protonated and can act as a H-bond donor. (**B**) The R_1-group influences the preferred tautomeric state and conformation. As an example, the lowest energy conformations (in solution) of the highly active compound **3d** and of the poorly active compound **3l** are shown here. Compound **3d** prefers the active conformation with tautomer A and **3l** exists in the inactive conformation with tautomer B.

Obviously, the preference of a specific tautomeric state does not fully determine the compound activity. For example, the inactive compound **3g**, clearly prefers tautomer A (86.9%), but the pyrimidine group is suboptimal for the hydrophobic region (solvent preference). On the contrary, the highly lipophilic *para*-fluorophenyl substituent in compound **1** clearly increases potency, despite its preference for tautomer B. Interestingly, the inactive 2-methoxyphenyl derivative **3f** appears only in a specific conformation as a tautomer A, wherein the methoxy-group folds on top of the pyridinyl ring (*Table S3*), which most likely impedes the binding. Overall, the tautomeric state preference partially, but not solely, determines the 2-methylimidazole activity.

Next, we attempted to improve the binding affinity of **1** via enhancing interactions at the solvent interface in the HR II. To this end, MD simulations (200 ns) demonstrated the potential suitability of compounds bearing *N*-(pyridin-2-yl)tri- or tetrazolepropanamide moieties (**4a**,**b**; *Figures S2–S4, SI*). Both displayed cation-π interactions with the Arg141 and improved solvent interactions combined with significantly lower log P values (*Table 2*) (*see SI for synthetic details*). The simulation of **4a** highlighted an identical binding mode for the triazole ring as observed in a crystal structure (PDB ID: 5K5N).[21]

Table 1. Activity and Physicochemical Parameters of 2-Methylimidazoles 3a-o.

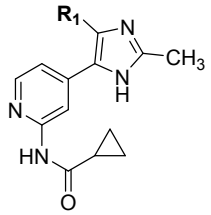

Cpd	R_1	IC_{50} ± SEM [μM] GSK3β[a]	IC_{50} ± SEM [μM] p38α MAPK	Alog P[b]	LLE	Tautomer A population (%)[c d]
1	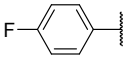	0.053 ± 0.012[d]	0.019[d,e]	2.88	4.40	29.386
2		1.68 ± 0.12[d]	>10[d,e]	0.72	5.10	n.d.[f]
3a	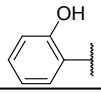	0.011 ± 0.001	0.050	2.40	5.56	85.508
3b	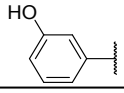	0.043 ± 0.005	0.024	2.40	4.97	2.834 (93.885[g])
3c	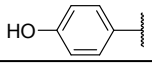	0.893 ± 0.001	1.851	2.40	3.65	12.687
3d		0.069 ± 0.000	0.048	2.40	4.77	81.318
3e		0.099 ± 0.033	0.987	1.84	5.17	71.467
3f	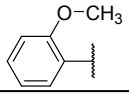	>10	0.504	2.65	-	31.19
3g		>10	>10	0.89	-	85.892
3h	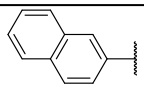	>10	0.081	3.58	-	20.289
3i	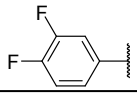	0.059 ± 0.007	0.019	3.08	4.15	n.d.[f]
3j		3.09 ± 0.30	>10	1.76	3.75	6.014
3k		4.11 ± 0.19	>10	2.22	3.17	10.229
3l		5.46 ± 0.01	>10	2.68	2.59	16.734
3m		4.64 ± 1.16	>10	3.13	2.20	16.552
3n	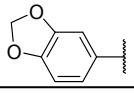	0.467 ± 0.006	0.030	2.44	3.89	n.d.
3o	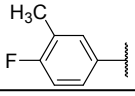	0.117 ± 0.015	0.007	3.36	3.57	n.d.

[a]n=2; [b]calculated with Canvas (Schrödinger LLC)[22]; [c]according to QM Conformer & Tautomer Predictor of Maestro (Schrödinger, LLC, New York, NY, 2018) (*see SI and Table S3 for details*); [d]values taken from Heider *et al.*[12]; [e]determined by ELISA activity assay[23]; [g]the intramolecular H-bond to amide conformation excluded (*see Table S3*); [f]n.d. = not determined.

Table 2. Activity and Physicochemical Parameters of *N*-(pyridin-2-yl)tri- or tetrazolepropanamide bearing 2-Methylimidazoles 4a-d.

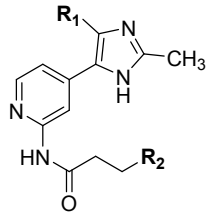

Cpd	R_1	R_2	IC_{50} ± SEM [µM] GSK3β[a]	IC_{50} ± SEM [µM] p38	Alog P[b]	LLE
4a	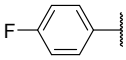		0.082 ± 0.007	0.041	1.16	5.92
4b	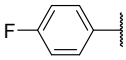		0.072 ± 0.008	0.038	1.83	5.32
4c			5.18 ± 0.10	>10	-0.99	6.27
4d			4.42 ± 0.29	>10	-0.32	5.65

[a]n=2; [b]calculated with Canvas (Schrödinger LLC)[22].

Compounds **4a** and **4b** show a similar potency as the lead compound **1** but with enhanced LLE values. Removal of the *para*-fluorophenyl anchor resulted in compounds **4c** and **4d**, both displaying substantially reduced inhibitory potency. This clearly results from the negative log P values of these compounds, which seems to compromise their binding affinity (entropic penalty). Nevertheless, these compounds still exhibit mediocre target inhibition and fit nicely into the SAR of the series.

To overcome the highlighted tautomerism-related issues observed with the 2-methylimidazoles, we designed and synthesized a series of imidazole-2-carboxamides. Instead of the acceptor nitrogen of tautomer A, the 2-carboxamides could neglect the tautomeric state of the imidazole by presenting the amide oxygen towards the Lys85 region. This amino acid side chain has been successfully targeted by carbonyl groups, e.g. Pfizer disclosed 6-amino-4-(pyrimidin-4-yl)pyridones interacting with Lys85,[24] while Bristol-Myers Squibb reported potent pyrrolopyridinones.[25] Moreover, we investigated ethyl esters as well as a hydroxyl moiety for their suitability to address the Lys85 residue.

In contrast to methylimidazole **2**, imidazole2-carboxamide **6a** showed a >35-fold improvement in potency (LLE 7.49) (*Table 2*). In case of compound **1**, the introduction of a carboxamide moiety at the imidazole-C2 position (**6h**) did not substantially improve the inhibitory activity. Installation of an ethyl ester (**5a** and **5c**) yielded mediocre inhibitors highlighting the importance of the amide function. Introduction of a hydroxy moiety at the imidazole-C2 methyl group resulted in **6i** showing a two-fold reduction in GSK3β inhibition and no shift in the IC_{50} value of p38α MAPK. In most cases, imidazole-2-carboxamides were better inhibitors of GSK3β than their corresponding 2-methylimidazole counterparts (e.g. **6c** vs **3f**, **6e** vs **3o**). Only the already potent 2-hydroxyphenyl **3a** (vs **6b**) displayed no improvement in activity.

The most striking differences existed in cycloalkyl substituted compounds **6f** and **6g** exhibiting dramatically improved potency against GSK3β along with higher LLE values compared to the corresponding 2-methylimidazole derivatives **3m** and **3j**, which displayed only mediocre activities and preferred the tautomer B. Moreover, all three compounds showed significant selectivity over p38α MAPK, and compound **6g** was among the best from this series (GSK3β, IC_{50}: 0.003 µM; p38α MAPK, IC_{50}: >10 µM; LLE 7.64).

To further investigate these dramatic activity differences, we first confirmed that the amide group replacing the methyl group on the imidazole-C2 position had no influence on the tautomeric state preference (*Table S3*). As an example, the cyclopropyl-substituted compounds **3j** and **6g** display an analogous population of the tautomeric state A, namely 6.0% and 6.7% for **3j** and **6g**, respectively. Nevertheless, the potency of these two inhibitors is dramatically different, with the imidazole-2-carboxamide derivative **6g** showing a three order of magnitude higher activity than its methyl counterpart (**3j**).

To gain a deeper insight into the compound binding and the activity differences between 2-methylimidazoles and imidazole-2-carboxamides, we conducted a total of 8 µs MD simulations for the selected compounds bound to GSK3β in their preferred tautomeric state: **3j** and **6g** in tautomeric state B and the **3a** and **6b** in tautomeric state A. The initial 1 µs MD simulations suggested unstable binding only for **3j**, where its lipophilic cyclopropyl group is exposed to water in HR-I (*Figure 3 and Figures S5 and S9, SI*). Whereas with **6g** the amide stabilizes a water network near Asp200 and the cyclopropyl group is shielded from the solvent allowing the stable binding of tautomer B (*Figure 3 and Figures S5 and S9, SI*). With tautomer A preferring **3a** and **6b**, the 2-hydroxyphenyl was shielded from solvent regardless of the methyl or amide group substituent in the imidazole ring (*Figure 3 and Figures S7 and S9, SI*). These observations

were confirmed in unbiased simulations, conducted using another crystal structure as the starting configuration (*Figures S6, S8 and S10, SI*). Based on these data, the energetically favorable tautomer B of **3j** does not support the suggested stabilizing interactions with the dynamic water network, which leads to water exposed HR-I, whereas the preferred tautomer A of **3a** is capable to shield the HR-I from water via direct or water mediated interactions to Lys85 and maintain a stable binding (*Figures S5–S8, SI*). Thus, QM calculations with the MD simulations provide a potential explanation for the observed activity differences.

Table 3. Inhibition Data and Physicochemical Parameters of Ethyl Imidazole-2-carboxylates 5 and Imidazole-2-carboxamides 6-8.

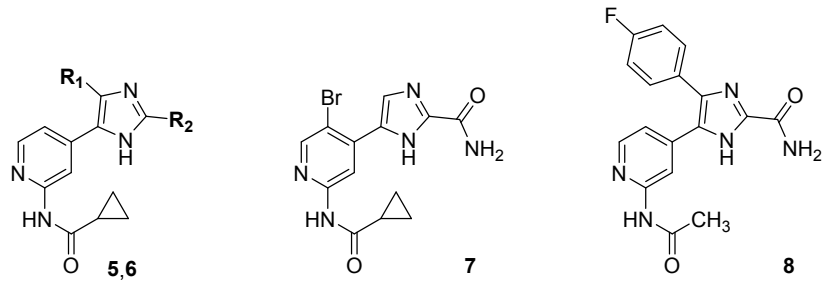

Cpd	R_1	R_2	IC_{50} ± SEM [µM] GSK3β[a]	IC_{50} ± SEM [µM] p38α MAPK	Alog P[b]	LLE
5a	H	O, O, CH_3	0.739 ± 0.186	>10	1.07	5.06
6a	H	O, NH_2	0.047 ± 0.020	>10[c]	-0.16	7.49
5c	F	O, O, CH_3	0.899 ± 0.010	0.089	3.23	2.82
6h	F	O, NH_2	0.039 ± 0.017	0.019 ± 0.002[c]	1.99	5.52
6i	F	OH	0.091 ± 0.006	0.016	2.20	4.84
6j	H_3C	O, NH_2	0.013 ± 0.001	>10	0.12	7.76
6g		O, NH_2	0.003 ± 0.000	>10	0.88	7.64
6f		O, NH_2	0.003 ± 0.000	>10	2.25	6.27
6b	OH	O, NH_2	0.023 ± 0.001	0.158	1.52	6.12
6c	O−CH_3	O, NH_2	0.265 ± 0.017	2.35	1.77	4.81
6e	H_3C, F	O, NH_2	0.079 ± 0.003	0.016	2.48	4.62
6d	F_3C−O	O, NH_2	0.352 ± 0.002	2.04	3.91	2.54
7	-	-	0.354[d]	>10	0.59	5.86
8	-	-	0.047 ± 0.004	0.117	1.24	6.09

[a]n=2; [b]calculated with Canvas (Schrödinger LLC)[22]; [c]determined by ELISA activity assay[23]; [d]n=1 .

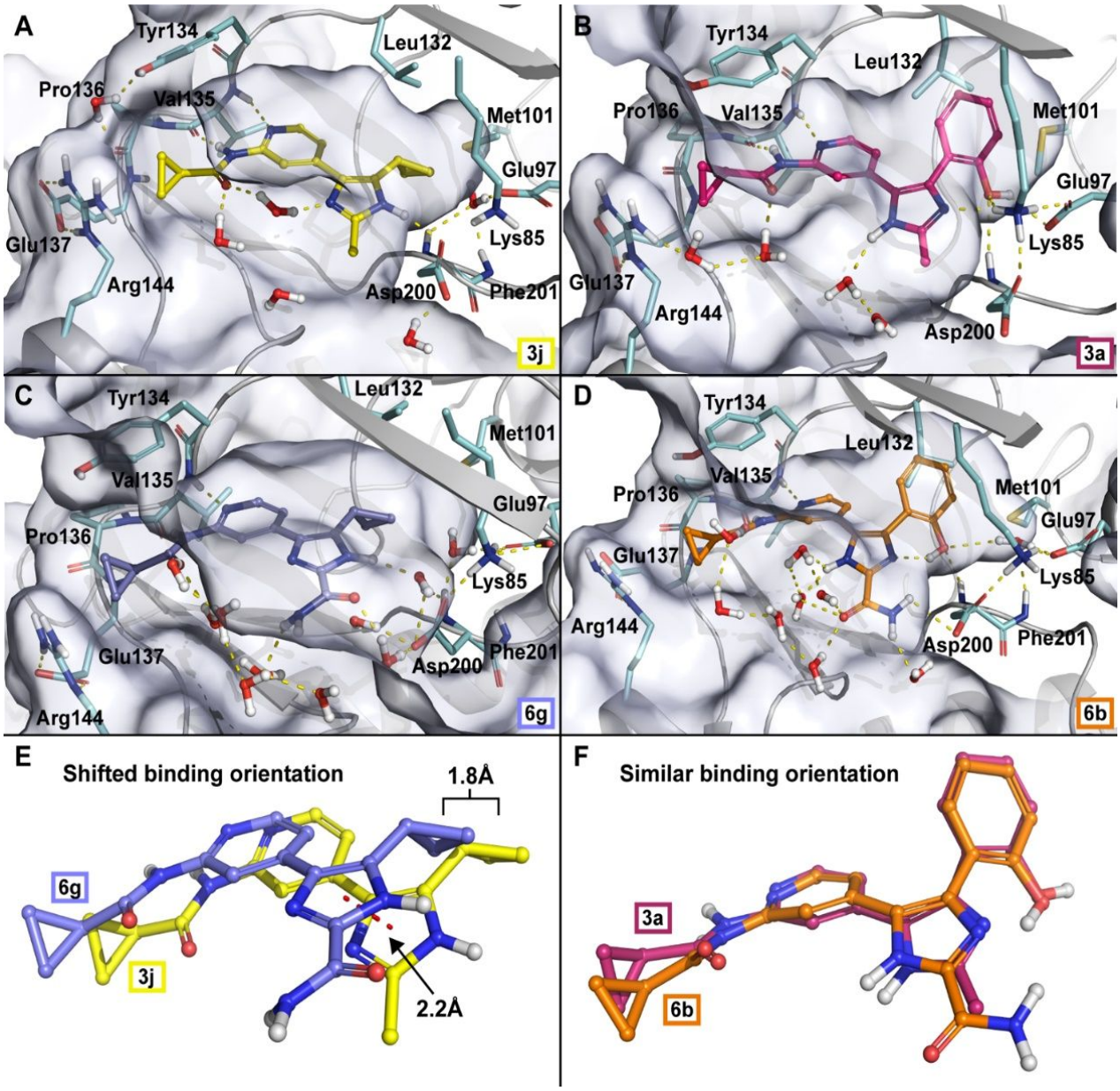

Figure 3. Representative snapshots from MD simulations of compounds **3i** (**A**), **3a** (**B**), **6g** (**C**) and **6b** (**D**). (**E**) Compound **3i** appears in a shifted binding orientation compared to **6g**, whereas both 2-hydroxyphenyl derivatives (**F**) **3a** and **6b** display similar binding orientation in the simulations. The shift in the binding orientation of compound **3j** occurs due to direct H-bond interaction from the imidazole to Asp200. This interaction, with the increased solvent exposure of the lipophilic cyclopropyl group (*see Figures S5–S6, SI*), explains the three orders of magnitude difference in activity between **3j** and **6g**. The protein surface is illustrated in transparent light blue color and hydrogen bonds with yellow dashed lines in **A-D**.

Selected compounds (**1**, **3a**, **3i**, **6a** and **6h**) were further tested for their GSK3β affinity in a previously reported ESI-QTOF assay (*Tables S1* and *S2, SI*).[26] Using this completely different assay system, the potency trend of these GSK3β inhibitors obtained in the ADP-Glo activity assay was confirmed.

Moreover, inhibitors **3a** and **6g** were tested for their metabolic stability by incubation with human liver microsomes (HLM) over a period of 4 h (*Tables S4* and *S5, SI*). Both compounds displayed excellent metabolic stability in this assay.

Further pharmacological profiling of the potent GSK3β inhibitor **6g** included the evaluation of its ability to inhibit relevant CYP isoforms (*Table 4*). At a test concentration of 10 μM, imidazole-2-carboxamide **6g** shows a clean CYP inhibition profile. Only low inhibition of CYP1A2 was observed.

Table 4. Inhibition of CYP450 isoenzymes.

	% inhibition of CYP isoform @ 10 μM				
Cpd	**1A2**	**2C9**	**2C19**	**2D6**	**3A4**
6g	25.5	0.8	-2.0	-2.8	-2.3

To assess the overall kinome selectivity, most promising inhibitor **6g** was screened against a representative panel of 68 diverse kinases (*Table S6, SI*), including the target kinase GSK3β and all members of the MAP kinases. At a concentration of 0.5 μM (>160-fold its IC_{50} value on the target kinase) only CDK2, CDK9, JNK3, MLK2 and VEGFR2 were substantially inhibited, suggesting an acceptable kinome selectivity.

To confirm the biological activity of imidazole-2carboxamide **6g**, we tested it in a cell-based GSK3β assay. At the tested concentration of 1 μM, **6g** inhibits GSK3β activity, in terms of inactive phospho-GSK3α/β (Ser21/9) increase, after 1 h of treatment in neuronal SH-SY5Y cells (*Figure 4*).

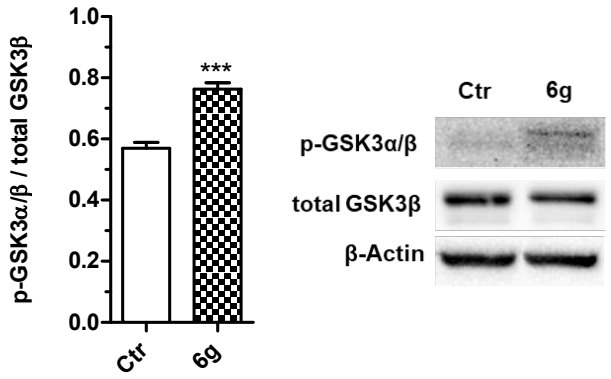

Figure 4. Inhibition of GSK3β activity in neuronal SH-SY5Y cells. Cells were incubated with compound **6g** [1 μM] for 1 h. At the end of incubation, the phosphorylation of GSK3α/β (Ser21/9) (inactive GSK3α/β form) was determined by western blotting. Data are expressed as ratio between phospho-GSK3α/β and total GSK3β levels normalized against β-Actin and reported as mean ± SD of at least three independent experiments (*** $p < 0.001$ versus untreated cells; t-test).

Since CDK2, CDK9 and VEGFR2 are off-targets of **6g**, we also determined its cytotoxic profile on different cell lines after 48 h of incubation. A margin of safety is given concerning cytotoxic side effects. In case of tested non-tumorigenic cells, the concentration to cause a 50% decrease in cell viability is in the low micromolar range, which corresponds >1000-fold the IC_{50} value of the GSK3β kinase activity assay (*Figure S11, SI*).

In case of the selected tumorigenic cells (*Figure S12, SI*), compound **6g** shows antiproliferative activity in breast human cancer cell line (*Figure S12B, SI*), at 0.1 μM and less at 0.01 μM. This may be a relevant result, as the GSK3β is a target in the treatment of human breast cancer.[27] Breast cancer patients with overexpression of GSK3β presented poor prognosis, and GSK3β inhibition suppressed the viability and proliferation of breast cancer cells in vitro.[28]

In summary, we synthesized a diverse set of 33 novel di- and trisubstituted pyridinylimidazoles. The most potent GSK3β inhibitors **6f**, **6g** and **6j** were selective over p38α MAPK and had reasonable (CNS) drug-like log P values. Imidazole **6g** was metabolically stable in HLM, displayed a very good selectivity profile, and showed no affinity towards pharmacologically relevant CYP isoenzymes. Importantly, the LLE values of the series illustrate that the series' potency is not driven by molecular obesity.[29]

The SAR of the synthesized compounds was explained with QM calculations and MD simulations. The series represent an interesting example of the influence of the 2-methylimidazole tautomerism on the compound activity. The effect of tautomerism was indirectly surmounted by introducing the water-network stabilizing 2-carboxamide, thus, exemplifying the importance to consider that subtle molecular differences may have significant influence on the dynamics of the system.

ASSOCIATED CONTENT

Supporting Information

The Supporting Information is available free of charge on the ACS Publications website.

Experimental details for preparation of the compounds; ESI-QTOF assay; cell-based GSK3β assay; molecular modeling, QM calculations and MD simulations; metabolic stability in HLM; kinome selectivity screening; inhibition of CYP450 isoenzymes; cell toxicity data (PDF).
QM output conformations, MD movies and full raw trajectories are freely available at https://doi.org/10.5281/zenodo.3362889.

AUTHOR INFORMATION

Corresponding Author

*pierre.koch@uni-tuebingen.de (Pierre Koch)

ORCID

Fabian Heider: https://orcid.org/0000-0003-2472-2457
Tatu Pantsar: https://orcid.org/0000-0002-0369-2909
Letizia Pruccoli: https://orcid.org/0000-0002-0739-2102
Andrea Tarozzi: https://orcid.org/0000-0001-7983-8575
Pierre Koch: https://orcid.org/0000-0003-4620-4650

Author Contributions

#F.H. and T.P. contributed equally to this work.

Notes

The authors declare no competing financial interest.

ACKNOWLEDGMENT

We thank Jens Strobach for his assistance in the p38α MAPK ADP Glo™ assay. The authors wish to acknowledge CSC – IT Center for Science, Finland, for computational resources. T.P. acknowledges the Orion Research Foundation sr for financial support.

ABBREVIATIONS

GSK, glycogen synthase kinase; HR, hydrophobic region; MAPK, MAP kinase; LLE, lipophilic ligand efficacy; MD, molecular dynamics; QM; quantum mechanics.

REFERENCES

1. Hooper, C.; Killick, R.; Lovestone, S., The GSK3 hypothesis of Alzheimer's disease. *J. Neurochem.* **2008**, *104*, 1433–1439.
2. Canter, R. G.; Penney, J.; Tsai, L.-H., The road to restoring neural circuits for the treatment of Alzheimer's disease. *Nature* **2016**, *539*, 187–196.
3. DaRocha-Souto, B.; Coma, M.; Perez-Nievas, B. G.; Scotton, T. C.; Siao, M.; Sanchez-Ferrer, P.; Hashimoto, T.; Fan, Z.; Hudry, E.; Barroeta, I.; Sereno, L.; Rodriguez, M.; Sanchez, M. B.; Hyman, B. T.; Gomez-Isla, T., Activation of glycogen synthase kinase-3 beta mediates β-amyloid induced neuritic damage in Alzheimer's disease. *Neurobiol. Dis.* **2012**, *45*, 425-37.
4. Rana, A. K.; Singh, D., Targeting glycogen synthase kinase-3 for oxidative stress and neuroinflammation: Opportunities, challenges and future directions for cerebral stroke management. *Neuropharmacology* **2018**, *139*, 124-136.
5. Eldar-Finkelman, H.; Schreyer, S. A.; Shinohara, M. M.; LeBoeuf, R. C.; Krebs, E. G., Increased glycogen synthase kinase-3 activity in diabetes- and obesity-prone C57BL/6J mice. *Diabetes* **1999**, *48*, 1662–1666.
6. Kitano, A.; Shimasaki, T.; Chikano, Y.; Nakada, M.; Hirose, M.; Higashi, T.; Ishigaki, Y.; Endo, Y.; Takino, T.; Sato, H.; Sai, Y.; Miyamoto, K.-I.; Motoo, Y.; Kawakami, K.; Minamoto, T., Aberrant glycogen synthase kinase 3β is involved in pancreatic cancer cell invasion and resistance to therapy. *PLoS One* **2013**, *8*, e55289.
7. Ugolkov, A. V.; Bondarenko, G. I.; Dubrovskyi, O.; Berbegall, A. P.; Navarro, S.; Noguera, R.; O'Halloran, T. V.; Hendrix, M. J.; Giles, F. J.; Mazar, A. P., 9-ING-41, a small-molecule glycogen synthase kinase-3 inhibitor, is active in neuroblastoma. *Anti-Cancer Drugs* **2018**, *29*, 717–724.
8. Yoshino, Y.; Ishioka, C., Inhibition of glycogen synthase kinase-3 beta induces apoptosis and mitotic catastrophe by disrupting centrosome regulation in cancer cells. *Sci. Rep.* **2015**, *5*, 13249.
9. Lovestone, S.; Killick, R.; Di Forti, M.; Murray, R., Schizophrenia as a GSK-3 dysregulation disorder. *Trends Neurosci.* **2007**, *30*, 142–149.
10. Jope, R. S.; Roh, M.-S., Glycogen Synthase Kinase-3 (GSK3) in Psychiatric Diseases and Therapeutic Interventions. *Curr. Drug Targets* **2006**, *7*, 1421–1434.
11. Marsell, R.; Sisask, G.; Nilsson, Y.; Sundgren-Andersson, A. K.; Andersson, U.; Larsson, S.; Nilsson, O.; Ljunggren, O.; Jonsson, K. B., GSK-3 inhibition by an orally active small molecule increases bone mass in rats. *Bone* **2012**, *50*, 619–627.
12. Heider, F.; Ansideri, F.; Tesch, R.; Pantsar, T.; Haun, U.; Döring, E.; Kudolo, M.; Poso, A.; Albrecht, W.; Laufer, S. A.; Koch, P., Pyridinylimidazoles as dual glycogen synthase kinase 3β/p38α mitogen-activated protein kinase inhibitors. *Eur. J. Med. Chem.* **2019**, *175*, 309-329.
13. Crespo, A.; Rodriguez-Granillo, A.; Lim, V. T., Quantum-Mechanics Methodologies in Drug Discovery: Applications of Docking and Scoring in Lead Optimization. *Curr. Top. Med. Chem.* **2017**, *17*, 2663–2680.
14. Zhou, T.; Huang, D.; Caflisch, A., Quantum Mechanical Methods for Drug Design. *Curr. Top. Med. Chem.* **2010**, *10*, 33–45.
15. Spyrakis, F.; Ahmed, M. H.; Bayden, A. S.; Cozzini, P.; Mozzarelli, A.; Kellogg, G. E., The Roles of Water in the Protein Matrix: A Largely Untapped Resource for Drug Discovery. *J. Med. Chem.* **2017**, *60*, 6781–6827.
16. Krimmer, S. G.; Cramer, J.; Betz, M.; Fridh, V.; Karlsson, R.; Heine, A.; Klebe, G., Rational Design of Thermodynamic and Kinetic Binding Profiles by Optimizing Surface Water Networks Coating Protein-Bound Ligands. *J. Med. Chem.* **2016**, *59*, 10530–10548.
17. Ganesan, A.; Coote, M. L.; Barakat, K., Molecular dynamics-driven drug discovery: leaping forward with confidence. *Drug Discovery Today* **2017**, *22*, 249–269.
18. Pantsar, T.; Poso, A., Binding Affinity via Docking: Fact and Fiction. *Molecules* **2018**, *23*, 1899.
19. Leeson, P. D.; Young, R. J., Molecular Property Design: Does Everyone Get It? *ACS Med. Chem. Lett.* **2015**, *6*, 722–725.
20. Hopkins, A. L.; Keserü, G. M.; Leeson, P. D.; Rees, D. C.; Reynolds, C. H., The role of ligand efficiency metrics in drug discovery. *Nat. Rev. Drug Discovery* **2014**, *13*, 105–121.
21. Liang, S. H.; Chen, J. M.; Normandin, M. D.; Chang, J. S.; Chang, G. C.; Taylor, C. K.; Trapa, P.; Plummer, M. S.; Para, K. S.; Conn, E. L.; Lopresti-Morrow, L.; Lanyon, L. F.; Cook, J. M.; Richter, K. E. G.; Nolan, C. E.; Schachter, J. B.; Janat, F.; Che, Y.; Shanmugasundaram, V.; Lefker, B. A.; Enerson, B. E.; Livni, E.; Wang, L.; Guehl, N. J.; Patnaik, D.; Wagner, F. F.; Perlis, R.; Holson, E. B.; Haggarty, S. J.; El Fakhri, G.; Kurumbail, R. G.; Vasdev, N., Discovery of a Highly Selective Glycogen Synthase Kinase-3 Inhibitor (PF-04802367) That Modulates Tau Phosphorylation in the Brain: Translation for PET Neuroimaging. *Angew. Chem. Int. Ed.* **2016**, *55*, 9601–9605.
22. Ghose, A. K.; Viswanadhan, V. N.; Wendoloski, J. J., Prediction of Hydrophobic (Lipophilic) Properties of Small Organic Molecules Using Fragmental Methods: An Analysis of ALOGP and CLOGP Methods. *J. Phys. Chem. A* **1998**, *102*, 3762–3772.
23. Goettert, M.; Graeser, R.; Laufer, S. A., Optimization of a nonradioactive immunosorbent assay for p38α mitogen-activated protein kinase activity. *Anal. Biochem.* **2010**, *406*, 233-234.
24. Coffman, K.; Brodney, M.; Cook, J.; Lanyon, L.; Pandit, J.; Sakya, S.; Schachter, J.; Tseng-Lovering, E.; Wessel, M., 6-amino-4-(pyrimidin-4-yl)pyridones: novel glycogen synthase kinase-3β inhibitors. *Bioorg. Med. Chem. Lett.* **2011**, *21*, 1429–1433.
25. Sivaprakasam, P.; Han, X.; Civiello, R. L.; Jacutin-Porte, S.; Kish, K.; Pokross, M.; Lewis, H. A.; Ahmed, N.; Szapiel, N.; Newitt, J. A.; Baldwin, E. T.; Xiao, H.; Krause, C. M.; Park, H.; Nophsker, M.; Lippy, J. S.; Burton, C. R.; Langley, D. R.; Macor, J. E.; Dubowchik, G. M., Discovery of new acylaminopyridines as GSK-3 inhibitors by a structure guided in-depth exploration of chemical space around a pyrrolopyridinone core. *Bioorg. Med. Chem. Lett.* **2015**, *25*, 1856–1863.
26. De Simone, A.; Fiori, J.; Naldi, M.; D'Urzo, A.; Tumiatti, V.; Milelli, A.; Andrisano, V., Application of an ESI-QTOF method for the detailed characterization of GSK-3β inhibitors. *J. Pharm. Biomed. Anal.* **2017**, *144*, 159-166.
27. Ugolkov, A.; Gaisina, I.; Zhang, J. S.; Billadeau, D. D.; White, K.; Kozikowski, A.; Jain, S.; Cristofanilli, M.; Giles, F.; O'Halloran, T.; Cryns, V. L.; Mazar, A. P., GSK-3 inhibition overcomes chemoresistance in human breast cancer. *Cancer Lett.* **2016**, *380*, 384-392.
28. Walz, A.; Ugolkov, A.; Chandra, S.; Kozikowski, A.; Carneiro, B. A.; O'Halloran, T. V.; Giles, F. J.; Billadeau, D. D.; Mazar, A. P., Molecular Pathways: Revisiting Glycogen Synthase Kinase-3β as a Target for the Treatment of Cancer. *Clin. Cancer Res.* **2017**, *23*, 1891-1897.
29. Hann, M. M., Molecular obesity, potency and other addictions in drug discovery. *MedChemComm* **2011**, *2*, 349.

For Table of Contents Use Only

Pyridinylimidazoles as GSK3β inhibitors: the impact of tautomer-ism on compound activity via water networks

Fabian Heider, Tatu Pantsar, Mark Kudolo, Francesco Ansideri, Angela De Simone, Letizia Pruccoli, Taiane Schneider, Marcia Inês Goettert, Andrea Tarozzi, Vincenza Andrisano, Stefan A. Laufer, Pierre Koch

Insert Table of Contents artwork here